Quantifying Magnitude Uncertainty of the 2019 Ridgecrest Earthquake Sequence Through a Sensitivity Study of the Relative Magnitude Method

Sydney L. Gable*[1] and Yihe Huang[1]

ABSTRACT

Precise knowledge of earthquake magnitudes is vital for accurate characterization of seismic hazards. However, the estimation of earthquake magnitude, particularly for small events, is complicated by differences in network procedures and completeness. This produces disparate magnitude estimates for the same event and emphasizes the need for a consistent and transportable magnitude estimation procedure. Here, we investigate the use of the relative magnitude method, which measures earthquake magnitude from a least-squares inversion of interlinked waveform amplitude ratios. Our results show that that the relative magnitude method can establish both local and moment magnitudes for many events in the 2019 Ridgecrest sequence. The method also provides constraints on moment magnitude estimates for M <3 events, which are not routinely available using current methods. Although the relative magnitude method is advantageous because it can be applied uniformly in various regions and does not require empirical distance or attenuation corrections, there are several parameters that require subjective decision making and may introduce bias in the resulting magnitude estimates. These include acceptable thresholds for signal-to-noise ratios and cross correlation, filtering procedures, sampling windows, and station selection. Here, we not only calculate magnitude but also investigate how the subjective decision making affects the resulting magnitudes. Based on our analysis, we present recommendations to enhance the utility of this method for future users.

KEY POINTS

- We use the relative magnitude method to recalculate local and moment magnitudes for the 2019 Ridgecrest earthquake sequence.
- We evaluate potential sources of bias introduced by subjective decision making for various input parameters.
- We present recommendations for procedures aimed at reducing uncertainty and variability of relative magnitude results.

Supplemental Material

INTRODUCTION

Magnitude is one of the most ubiquitous and important source parameters in any seismic network operation. Routine estimation of earthquake magnitudes by seismic networks is commonly characterized by local magnitude (M_L) for most, if not all, events. The M_L scale was first developed by Richter (1935) and adjusted afterward so that the peak amplitude is measured for a particular waveform and corrected for source–receiver distance and path attenuation. This method may be applied to all earthquakes measured at a particular station, and reported network M_L magnitudes are often the mean of M_L measurements across all available stations. However, amplitude measurements made for a particular frequency band are likely to be underestimated for large earthquakes that are not filtered appropriately. This is known as magnitude saturation (Howell, 1981).

Moment magnitude (M_w) is often the preferred magnitude measure because it is directly related to the seismic moment (M_0) and not subject to saturation (Kanamori, 1977). M_0 is

1. Department of Earth and Environmental Sciences, University of Michigan, Ann Arbor, Michigan, U.S.A., https://orcid.org/0000-0002-9516-1768 (SLG); https://orcid.org/0000-0001-5270-9378 (YH)

*Corresponding author: gablesyd@umich.edu

Cite this article as Gable, S. L., and Y. Huang (2024). Quantifying Magnitude Uncertainty of the 2019 Ridgecrest Earthquake Sequence Through a Sensitivity Study of the Relative Magnitude Method, *Bull. Seismol. Soc. Am.* **115**, 1294–1307, doi: 10.1785/0120240126

commonly measured from moment tensor inversions of long-period waves, which are not greatly affected by shallow structural variations (Ristau *et al.*, 2003). However, due to low signal-to-noise ratios (SNRs) of long-period waves, M_w is usually not estimated directly for small events (M <∼3; Edwards *et al.*, 2010; Atkinson *et al.*, 2014).

Previous studies have investigated the relationship between M_L and M_w for different regions (Hanks and Boore, 1984; Ristau, 2009; Bethmann *et al.*, 2011; Gasperini *et al.*, 2013). However, the estimation of both M_L and M_w by seismic networks often encounters systematic error that arises from the application of velocity models and distance corrections developed for very broad regions (Deichmann, 2006). This leads to uncertainty in magnitude estimates, which results in (1) differences in magnitude reported for a particular event as measured by multiple networks or methods (Shelly *et al.*, 2022; Gable and Huang, 2024a) and (2) differences between M_w and M_L for the same event, both of which are amplified for small earthquakes (M <3). Accurate estimations of magnitude are vital for computation of earthquake hazard statistics, such as the magnitude–frequency distribution and their resulting *a*- and *b*-values (e.g., Castellaro *et al.*, 2006; Herrmann and Marzocchi, 2021), understanding of catalog completeness (e.g., Woessner and Weimer, 2005), and the derivation of empirical ground-motion relationships (e.g., Bindi *et al.*, 2018). In each of these applications, differences in magnitude and incorrect merging of multiple magnitude types may bias the resulting analysis significantly. A common solution for problem (2) is to convert M_L to M_w for small events using an established conversion relationship for a particular region. However, scaling relationships between M_w and M_L are also biased due to a lack of M_w estimates for small events (Deichmann, 2017; Shelly *et al.*, 2022). Therefore, a reliable method of measuring M_w for a wide range of earthquake size, applicable to a variety of tectonic environments and geographic regions, is needed to solve both problems and establish routine earthquake magnitudes.

Relative measurements have been shown to improve upon the precision of certain earthquake source parameters including magnitude (Schaff and Richards, 2014) and location (Waldhauser and Ellsworth, 2000). We can use this idea to derive relative earthquake magnitudes for a catalog of events by measuring the relative amplitude differences between pairs of highly similar, interlinked waveforms (see the Methods section for more details). This method avoids traditional sources of error in distance and attenuation corrections by assuming that highly correlated events are located close together and share similar path effects. Thus, the difference in amplitudes between two waveforms is attributed to the difference in magnitudes of the two earthquakes.

The 2019 Ridgecrest, California, earthquake sequence is of particular interest for understanding seismic hazard in southern California due to the size of the earthquakes as well as the complexity of faulting and rupture processes. Despite being located in one of the most seismically active regions in Southern California (Cheng and Ben-Zion, 2020), the M_w 7.1 mainshock was the largest earthquake to occur in this region since 1999. The mainshock was followed by thousands of aftershocks (Shelly, 2020), and the sequence was found to rupture a set of unmapped orthogonal faults (Liu *et al.*, 2019). Fortunately, the density of instrumentation and data quality available in southern California has allowed for rich investigations into the source processes of these earthquakes including those that focus on stress drop (Trugman, 2020, Baltay *et al.*, 2024), seismic moment and moment tensors (Cheng *et al.*, 2021), and magnitude (Bindi *et al.*, 2021), as well as the effects of these source parameters on seismic hazard and ground-motion estimates (Kuehn and Abrahamson, 2018). The Ridgecrest sequence is particularly useful for this study due to its wide magnitude range and densely located earthquakes, leading to many interlinked pairs of events with high cross correlation (CC).

Although the relative magnitude method provides a valuable avenue for magnitude determination, there are a number of parameters that must be subjectively chosen, which include (but are not limited to) acceptable signal-to-noise ratio (SNR), minimum thresholds for acceptable CC, band-pass filtering range, and station selection. In this study, we explore the variability of relative magnitude estimates based on different choices of the aforementioned parameters. This allows us to establish moment magnitude estimates for small earthquakes, for which direct measurement is very difficult or impossible. In addition, we use these results to recommend procedures for future users of the relative magnitude method.

DATA

We apply the relative magnitude method to a template-matched catalog of 34,091 events developed by Shelly (2020). The catalog includes events that occur between 4 and 16 July 2019, which encompasses the main Ridgecrest sequence and early aftershock sequence (∼11 days after the mainshock), including a M 6.4 foreshock on 4 July 2019 followed by the M 7.1 mainshock on 5 July (Fig. 1). We download velocity waveforms for five selected stations (Fig. 1) from the Southern California Earthquake Data Center (SCEDC). These waveforms are demeaned, and 8 s signal windows are cut at 1 s before to 7 s after the theoretical *P*- and *S*-wave arrival times for the vertical and horizontal components, respectively. Similarly, noise windows for each waveform consist of 8 s of noise ending 5 s before the *P*-wave arrival. Station response is not removed because we only compare waveforms that are measured on the same station.

METHODS

Rather than measuring magnitude from the maximum amplitude and correcting for source–receiver distance and path

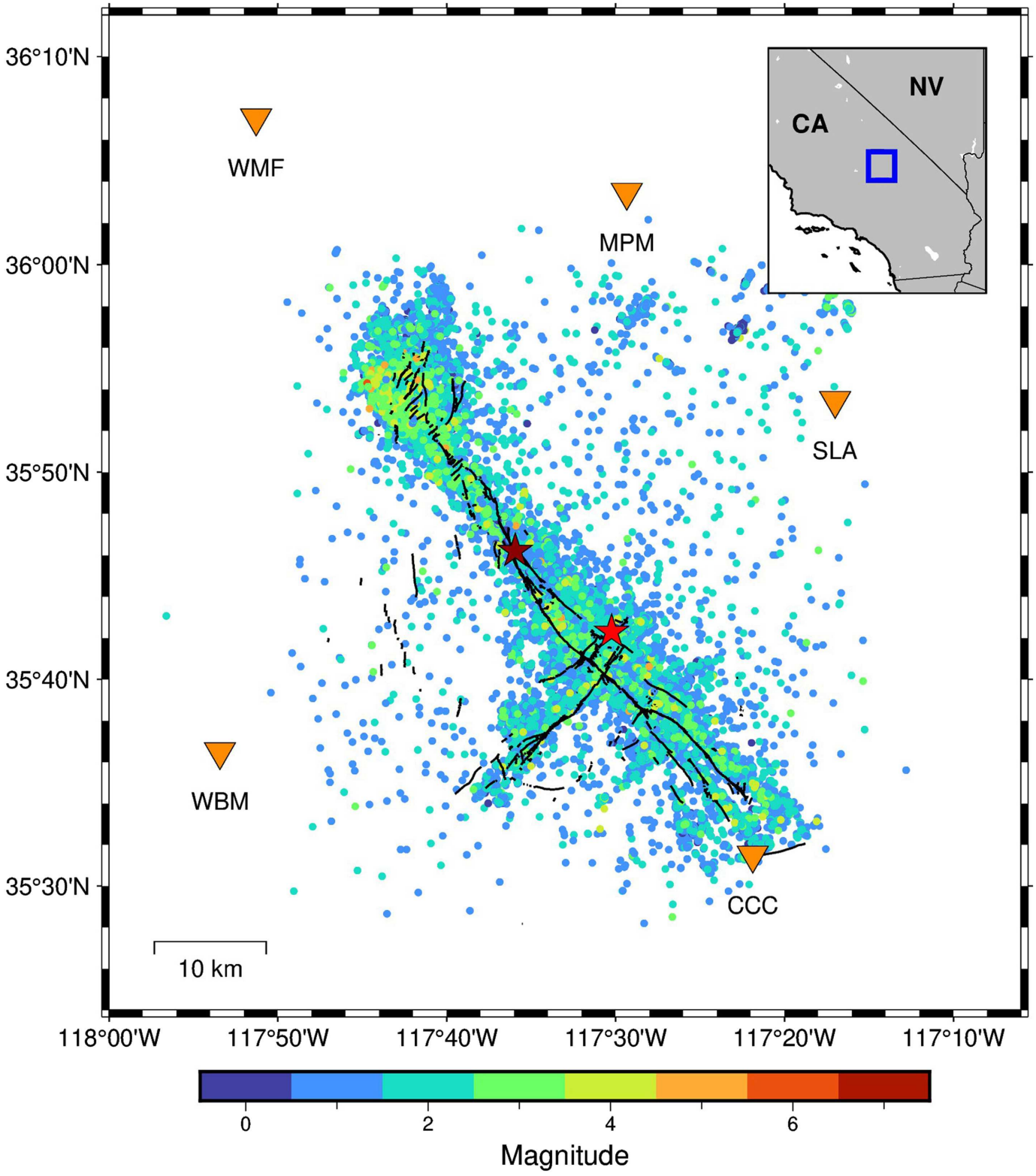

attenuation, this approach measures the amplitude ratios between many interlinked waveform pairs and utilizes a least-squares inversion to compute best-fit magnitudes for a group of events.

The relative magnitude method used here is modified from previous methods (Cleveland and Ammon, 2015; Gable and Huang, 2024a). For each waveform, we apply an SNR

Figure 1. Map of 2019 Ridgecrest Sequence events. Color of circles corresponds to magnitude as determined by Shelly (2020). Red and dark red stars represent locations of the M 6.4 foreshock and M 7.1 mainshock, respectively. Orange triangles represent stations used to calculate relative magnitudes. Black lines represent surface fault ruptures produced by the Ridgecrest sequence (Ponti *et al.*, 2020). Inset map shows the location of the Ridgecrest sequence in Southern California. The color version of this figure is available only in the electronic edition.

TABLE 1
Summary of Each of 24 Parameter Cases Including Changes of Frequency Band, CC Threshold, SNR Threshold, and Station Configuration

Case	Frequency Band (Hz)	CC Threshold	SNR Threshold	Station Configuration	Figure Reference
Base	0.5–12	0.6	3	Five stations	Figure 2
Case 1	0.5–12	0.6	5	Five stations	Figure 3
Cases 2–8	0.5–12	Varies between 0.45 and 0.8	3	Five stations	Figure 4
Cases 9–13	0.5–12	0.6	3	Four stations: one original station dropped in each case	Figure 5
Cases 14–18	0.5–12	0.6	3	One station per case	Figure 6
Case 19	0.5–12	0.6	3	Minimum three stations	Figure 7
Case 20	0.5–12	0.6	3	Minimum four stations	Figure 7
Case 21	0.5–12	0.6	3	Minimum five stations	Figure 7
Case 22	0.1–12	0.6	3	Five stations	Figure 8
Case 23	0.5–20	0.6	3	Five stations	Figure 8
Case 24	Magnitude-dependent frequency band (0.5–20 Hz for M <3.5, 0.1–12 Hz for M >3)	0.6	3	Five stations	Figure 8

CC, cross correlation; SNR, signal-to-noise ratio.

threshold test for which SNR is calculated by dividing the maximum amplitude of the signal window by the root mean square of the noise window. Waveforms with SNR less than the prescribed threshold are excluded from analysis. The resulting waveform pairs must then pass a CC threshold test (see Table 1 for SNR and CC threshold values used in this study). For each waveform pair that passes both tests, amplitude ratios are averaged across all channels (north–south, east–west, and vertical). Then, measurements for each event pair are also averaged across each available station. We require amplitude ratio measurements to be available from at least two stations and the events in each pair must be located within 0.2 arc degrees. This allows for averaging of potential measurement errors and reduces the required computational resources to carry out the inversion.

We measure the amplitude ratio (α) between two waveforms using the ratio of the elements of the largest eigenvector ($v1$ and $v2$) of the waveform's covariance matrix in the following equation (Shelly *et al.*, 2016):

$$\alpha = \frac{v_2}{v_1}. \tag{1}$$

The logarithm of the amplitude ratio times a scaling coefficient (c) then gives the difference between the magnitudes of the two events (M_1 and M_2) in the following equation:

$$M_2 = M_1 + c\log_{10}\alpha. \tag{2}$$

Previous studies have suggested different values for the scaling coefficient depending on magnitude type. Here, we calibrate the relative magnitudes using both local scaling and moment magnitude scaling. For local magnitudes M_L, previous studies (Huang and Beroza, 2015, Chen *et al.*, 2018) employ a scaling coefficient of 1 based on the expected direct scaling of waveform amplitude and local magnitude. When comparing our results to cataloged estimates of M_L, we also use a scaling factor of $c = 1$ to establish relative M_L. When comparing our results of relative M_w to cataloged M_w, we choose to use a magnitude scaling coefficient of ⅔ to reflect the expected scaling between earthquake moment and the logarithm of the waveform amplitude as local magnitude (or amplitude) versus logarithm of the seismic moment can be fit with a slope of 1.5 (Hanks and Boore, 1984, Cleveland and Ammon, 2015).

Once the final amplitude ratio is determined for each event pair, we can calculate the "best-fit" magnitudes (M_n) from a least-squares inversion in the following equation:

$$\begin{bmatrix} c\log_{10}\alpha_{1,2} \\ c\log_{10}\alpha_{1,3} \\ \cdots \\ c\log_{10}\alpha_{1,n} \\ M_{\mathrm{calib},1} \\ \cdots \\ M_{\mathrm{calib},i} \end{bmatrix} = \begin{bmatrix} 1 & 1 & -1 & 0 & \ldots & 0 & 0 \\ 1 & 1 & 0 & -1 & \ldots & 0 & 0 \\ 1 & \ldots & \ldots & \ldots & \ldots & \ldots & \ldots \\ 1 & 1 & 0 & 0 & \ldots & 0 & -1 \\ 1 & 1 & 0 & 0 & \ldots & 0 & 0 \\ 1 & \ldots & \ldots & \ldots & \ldots & \ldots & \ldots \\ 1 & 0 & 0 & 0 & \ldots & 0 & 0 \end{bmatrix} \times \begin{bmatrix} x \\ M_1 \\ M_2 \\ M_3 \\ \cdots \\ M_n \end{bmatrix}, \tag{3}$$

in which α_{mn} represents the amplitude ratio between events m and n, $M_{\mathrm{calib},i}$ represents the known magnitudes of a group of calibration magnitudes and x is a constant term in the least-squares inversion.

Previous methods (Cleveland and Ammon, 2015; Chen *et al.*, 2018; Kintner *et al.*, 2018, 2020) utilize the sum of the originally cataloged magnitudes (or moments) to scale the

results of the inversion from a dimensionless magnitude quantity to a moment magnitude scale. However, our motivation is to evaluate magnitudes assuming that ground-truth is unknown. Thus, we must also consider the total magnitude (or moment derived from the magnitudes) to be unknown as well. Therefore, we instead establish a catalog of calibration events with independently estimated M_w that is individually input in the inversion (equation 3). Using this method, we form links between calibration and measured events that calibrate the measured events to the moment magnitude scale without relying on knowledge of total earthquake moment. To calibrate the relative M_w estimates in this study, we use the 125 available moment magnitudes in the Southern California Seismic Network (SCSN) catalog. All events have M >3.5. For the relative M_L calibration, we use M_L estimates for the same 125 events, which are available from the U.S. Geological Survey (USGS; contributed by the CI network). Because this method is dependent on interlinking waveform pairs with at least one measured event linking to a calibration event, we recognize that a greater number of calibration magnitudes would provide more linkages and thus more relative magnitude results. However, we are not able to test a higher number of calibration magnitudes because we currently use all of the available moment magnitudes from the SCSN catalog. Future work may seek to independently establish a greater number of moment magnitudes to test the ideal number of calibration events.

We first establish a base case with waveform data from five broadband stations. We choose these stations based on azimuthal coverage, data quality, and distance to the centroid of the earthquake sequence. These five stations are located at distances greater than 0.25 arc degrees (chosen to include 95% of the earthquakes) to increase the opportunity to identify pairs with similar source–receiver paths. These stations are also located closer than two times the aforementioned radius (0.5 arc degrees) to ensure high-SNR quality. The waveforms are bandpass filtered to 0.5–12 Hz, and CC and SNR thresholds are set to be 0.6 and 3, respectively, based on prior use of this method (Gable and Huang, 2024a). With these parameters, we estimate relative M_L and M_w for the 2019 Ridgecrest sequence.

Once we establish a base set of magnitudes using the aforementioned input parameters (summarized in Table 1), we investigate the variability of the relative magnitude results by changing each input parameter (Table 1) and comparing the results in each new case to the base case.

RESULTS

Base case

With the base-case parameters, we estimate magnitude for 19,754 events (Fig. 2). We find that events with M >2 are more likely to be recalculated because many events with M <1.5 are excluded due to low SNR. In addition, we find that increased waveform complexity of large events (M >4.5) also prevents the formation of many highly correlated pairs.

We compare our results for both relative M_L and M_w from the base case with magnitude estimations published in various other catalogs (Fig. 2a–d). Bindi *et al.* (2021) estimate M_L from a calibrated local magnitude scale (Richter, 1935, Savage and Anderson, 1995) using the Urlhammer *et al.* (2011) attenuation function for California. This attenuation function is also used for the SCSN network magnitudes. Liu *et al.* follows a similar approach instead using the Hutton and Boore (1987) distance and attenuation correction formula for southern California. Shelly (2020), a template-matching study, estimates local magnitude for detected events by amplitude ratio comparison with template events that have a cataloged SCSN magnitude. This method is the most similar to ours because it utilizes amplitude ratio to establish magnitude differences between events. However, Shelly (2020) uses a scaling constant of 0.831 based on SCSN cataloged magnitudes and amplitude ratio measurements.

To quantitatively compare how our results agree with the previously cataloged estimates, we calculate the root mean square error (rmse) deviation between our relative magnitude results and other catalog results for each magnitude bin with width = 0.5 (Fig. 2a–e).

For M <3 events, our relative M_L is consistently lower than the cataloged estimates (with rmse values of 0.3–0.6) but agree the best with the Liu *et al.* (2020) M_L. For larger events (M >3), the Bindi catalog shows a consistent slope with the relative M_L but is biased to be larger than the relative M_L. We note that the Bindi catalog M_L is also consistently larger than the calibration event magnitudes. Thus, the disagreement between calibration magnitudes and Bindi catalog M_L is likely to lead to the bias between Bindi M_L and relative M_L. We also note a "turn-down" of the slope between cataloged M_L and relative M_L in Figure 2a–c. This could be the result of incorrect *c*-values in the matrix inversion. However, because this bias is not observed in the larger events, we attribute this to a difference in scaling between the small and large earthquakes. For M >3 events, we observe a higher level of agreement between cataloged M_L and relative M_L for the Shelly catalog as magnitude increases, whereas the level of agreement is fairly consistent as magnitude increases for the Bindi and Liu catalogs.

Finally, we observe the best agreement between our relative M_w and the Bindi *et al.* (2021) M_w estimates, although we cannot make any observations about M_w scaling at smaller magnitudes because cataloged estimates of M_w for small earthquakes are not available from the Bindi catalog or SCSN.

We also compare our results for relative M_L and M_w with each other and find that for M >3.5 events M_L and M_w agree well despite the different scaling constants used in the inversions (Fig. 2f). We apply an orthogonal regression to these events and find a best-fit line with a slope of 1.16, which is close to the expected slope of 1. For M <3.5 events, we observe that M_w is consistently higher particularly for the smallest events. The best-fit line for these events has a slope of 1.49.

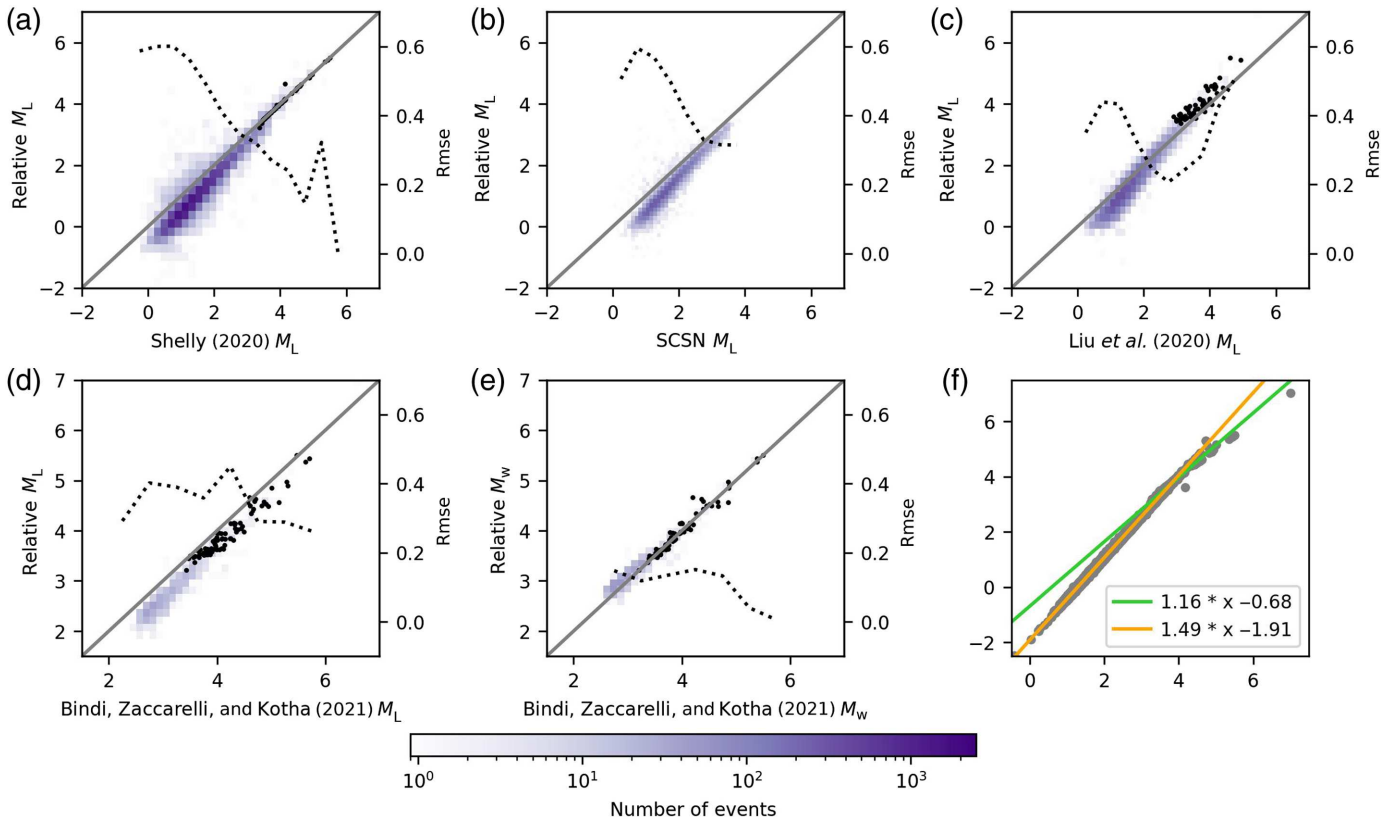

This is expected based on comparisons between moment and local magnitude in other tectonic regions (Deichmann, 2006; Edwards *et al.*, 2010; Ross *et al.*, 2016; Holt *et al.*, 2021). Given the consistency between relative M_L and M_w results, we focus on the relative M_w results next to explore the effects of input parameters of the relative magnitude method (Table 1). We compare the results of each inversion to the M_L estimates cataloged in Shelly (2020) because cataloged M_w is not available for most events.

Figure 2. (a–d) Results of base-case relative M_L inversion compared with other estimates of M_L for (a) the Ridgecrest Sequence, (b) the Southern California Seismic Network (SCSN) catalog, (c) Liu *et al.* (2020), and (d) Bindi *et al.* (2021). (e) Results of base-case relative M_w inversion compared with the Bindi *et al.* (2021) estimates of M_W for the Ridgecrest Sequence. For panels (a–e), black dots represent the comparison between catalog M_L or M_w and calibration events. Gray line represents a 1-to-1 relationship, and the black-dotted line represents the root mean square error (rmse) value as a function of magnitude bin. (f) Comparison between relative M_L results and relative M_w results generated using this method. The orange line is a best fit for M <3.5 events, and the green line fits M >3.5 events. The color version of this figure is available only in the electronic edition.

SNR

We first investigate the impact of raising the SNR threshold from 3, as in the base case, to 5 (case 1). We find that when raising the SNR threshold, the number of events included in the inversion is reduced from 19,584 to 15,531. Most events that are excluded from raising SNR have M <2. This suggests that very small events experience more noise contamination and are subsequently excluded when the SNR threshold is increased.

For the majority of events that are included in both inversions, there is not a significant difference between the relative M_w calculated in the base case and case 1 (Fig. 3b). In fact, 98.3% of events have a magnitude difference less than 0.05 between the base case and case 1 (SNR = 5). Furthermore, the comparison between base case and case 1 has an rmse values of 0.001. However, we can observe that the events with significant variation between the two cases are small events (M <2.5). This is evidenced by the difference between base case and case 1 results (Fig. 3b), which are much larger for smaller magnitudes. This suggests that the inclusion of the 4053 events with low SNR does not significantly affect the results of the other events. Therefore, we recognize that future choices for SNR may be dependent on the goal of the particular end user. A low SNR would allow for a higher number of events to be recalculated but potentially sacrifices the accuracy of the magnitude estimates for the smallest events likely due to waveform contamination by noise. We recommend a low SNR that ensures the highest number of events to be included as possible while minimizing potential contamination by noise that is very close to the amplitude of the earthquake signal. An SNR that is too low would cause very small magnitude events to be calculated at the magnitude of the noise level rather than the event amplitude itself and would be observed as a "leveling-off" of the relative magnitudes at the smallest end.

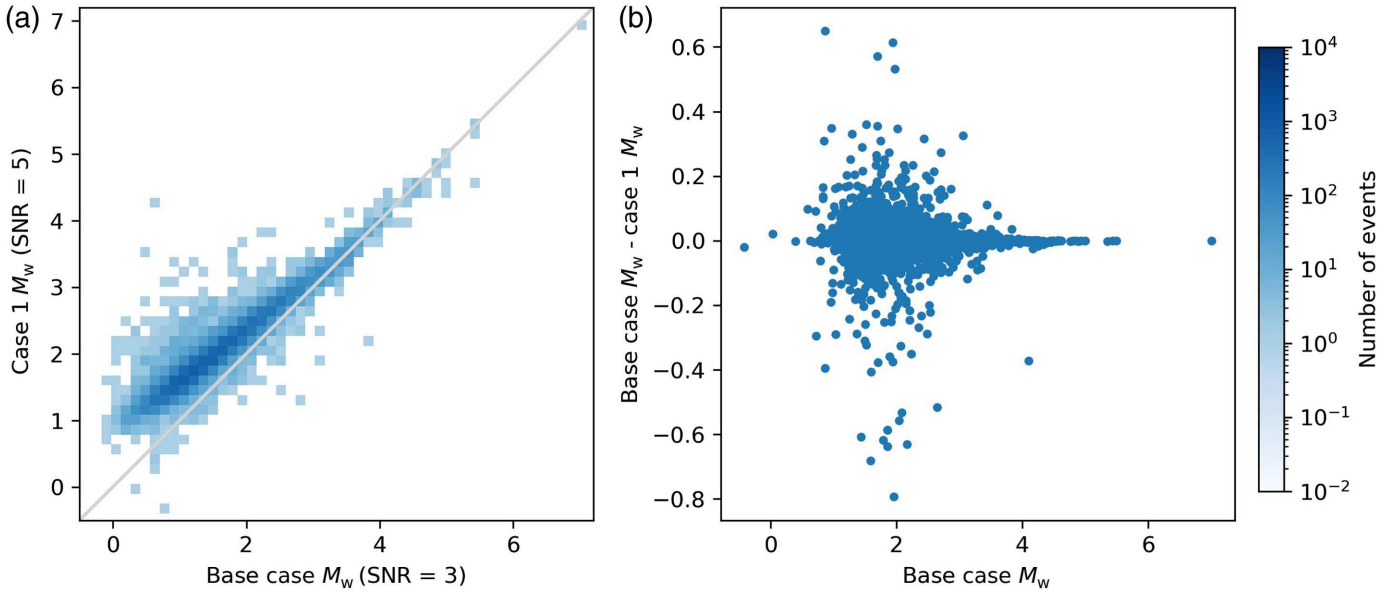

Figure 3. (a) Comparison of relative M_w results for the base case (signal-to-noise ratio [SNR] = 3) and case 1 (SNR = 5). The color of the histogram represents the number of events in the magnitude bin. The light-gray line represents a 1-to-1 relationship. (b) Difference between base-case M_w and case 1 M_w results compared to the base-case M_w value. The color version of this figure is available only in the electronic edition.

CC

Next, we examine the effects of varying the CC threshold between 0.45 and 0.8 (cases 2–8, Fig. 4). We also plot the differences between the base-case M_w and relative M_w results for each case to examine the variability as a function of magnitude (Fig. 4, inset plots).

Similar to the SNR test, lowering the CC threshold increases the number of pairs that are included in the inversion and consequently increases the number of events for which relative M_w is calculated. However, we find that for CC < 0.6, there are large differences between the base-case M_w and each case results particularly for M <2. This can be observed in both the main figures and inset points as the scatter in the data plots. This effect is likely due to the inclusion of events that are not closely located and do not share similar source–receiver paths, thus not ensuring that the amplitude difference faithfully reflects the difference in magnitude between the two events.

Conversely, raising the CC threshold would ensure that only the most highly correlated pairs are included in the inversion while sacrificing the number of events available. Once CC increases above 0.6, we observe a significant drop in the number of events included in the inversion (i.e., below 50% of the total number of events in the catalog). Although we can still effectively quantify the magnitude differences through the matrix inversion, the number of recalculated events is important particularly for the calibration of the inversion to an absolute scale and for the magnitude–frequency distribution.

When raising the CC threshold above 0.65, we begin to observe horizontal lineations in the differences between base-case M_w and the raised CC cases (cases 5–8). This is caused by the presence of distinct groups of events that share internal linkages to each other but are not interlinked to other groups. If these smaller groups contain only a small number or no calibration events, they will not be accurately calibrated with the rest of the catalog even though the magnitude differences within each group are evaluated accurately.

In addition, the lack of events pairs due to high-CC thresholds is a problem for the magnitude–frequency distribution because a deficiency of events in a particular magnitude range may influence the slope of the distribution, also known as the *b*-value. Here, we show that the magnitude–frequency distribution for CC = 0.45–0.55 are very similar, whereas a higher CC threshold (CC > 0.75) begins to lose 3 > M > 5 events disproportionately to the middle magnitudes. For the high-CC threshold cases (cases 5–8), disproportionate reduction in the number of small events would lead to an artificially low *b*-value. For future users, we would recommend not increasing the CC threshold above 0.65 or lowering below 0.5, unless the user is more concerned with accuracy of magnitude differences rather than statistical products that rely on a complete catalog.

Station selection

Next, we analyze the contributions of each individual station by systematically removing each station from the inversion. We compare the results of the base case to each case where a particular station is omitted (cases 10–13, Fig. 5). The contributions from each station are represented by the difference in relative M_w between the case where the station is dropped and the base case. Large differences signify that the results change significantly when the station is excluded and thus is important to constrain the inversion. Although all five cases exhibit similar results, we find that the cases where stations

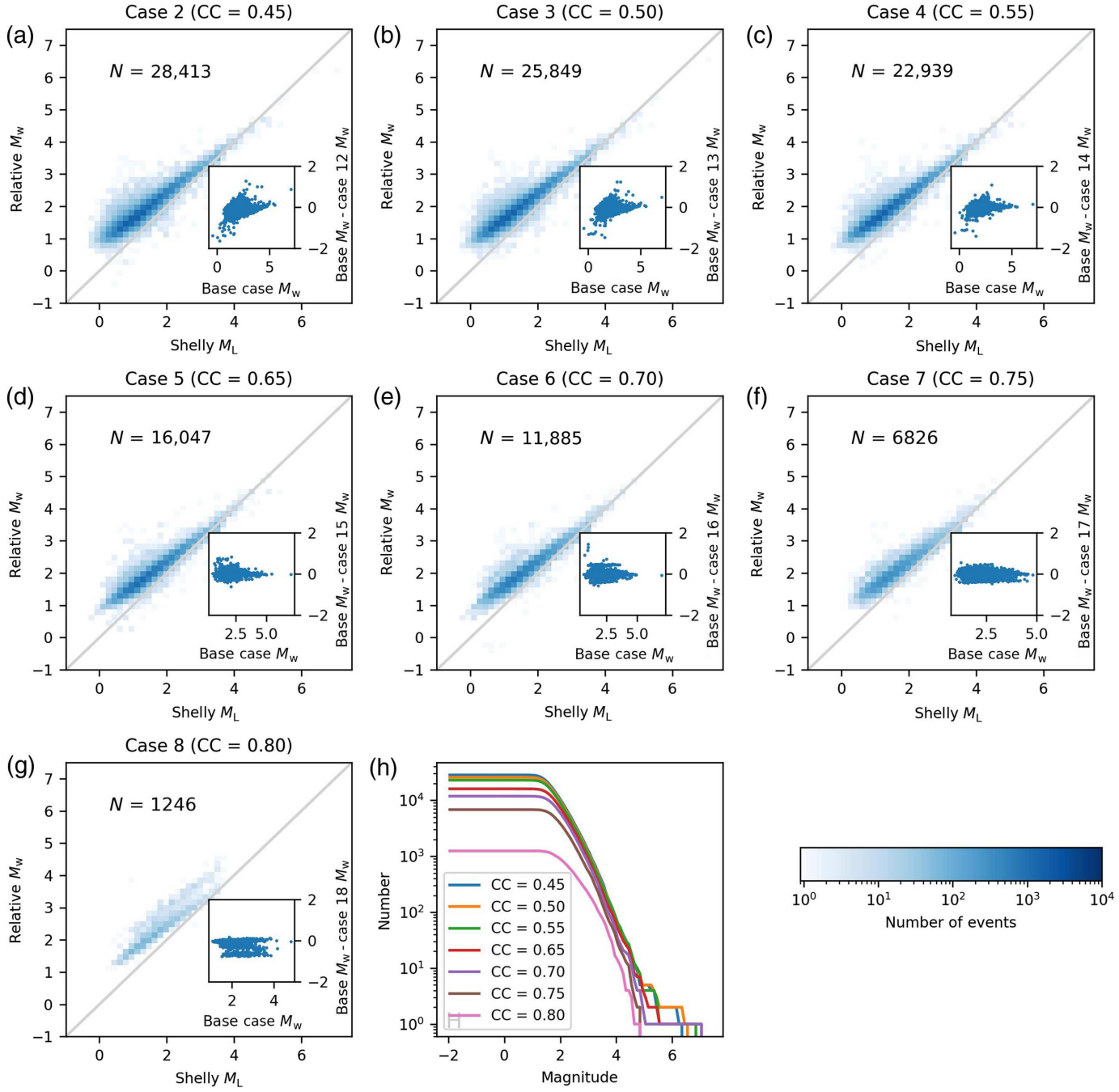

Figure 4. (a–g). Relative M_w compared to M_L cataloged by Shelly (2020) for seven cases with varying acceptable cross-correlation (CC) thresholds. Intensity of color represents the number of events in each magnitude bin. *N* represents the number of events that are calculated in each case. Inset plots show the difference between base-case M_w and relative M_w for each case compared to the base-case M_w alone. Panel (h) shows the distribution of recalculated relative M_w for each CC threshold case. The color version of this figure is available only in the electronic edition.

CCC and WMF are dropped (cases 9 and 13) exhibit the least scatter and retain the largest number of events. Therefore, the exclusion of these two stations impacts the variability of the final results the least compared to other stations. Interestingly, these two stations contribute the largest number of event pairs to the base case and are located along strike of the main fault. It is likely that the two along-strike stations contribute more event pairs because there are more event pairs that share similar paths, and thus high correlation for a station that lies along strike. However, the small differences between these two cases and the base-case results suggest that these stations are not as effective as other stations when constraining results.

Conversely, stations MPM and WBM (cases 11 and 12), which lie orthogonal to the main fault, show the largest differences from the base case when they are removed from the inversion. Although we do highlight the differences in scatter

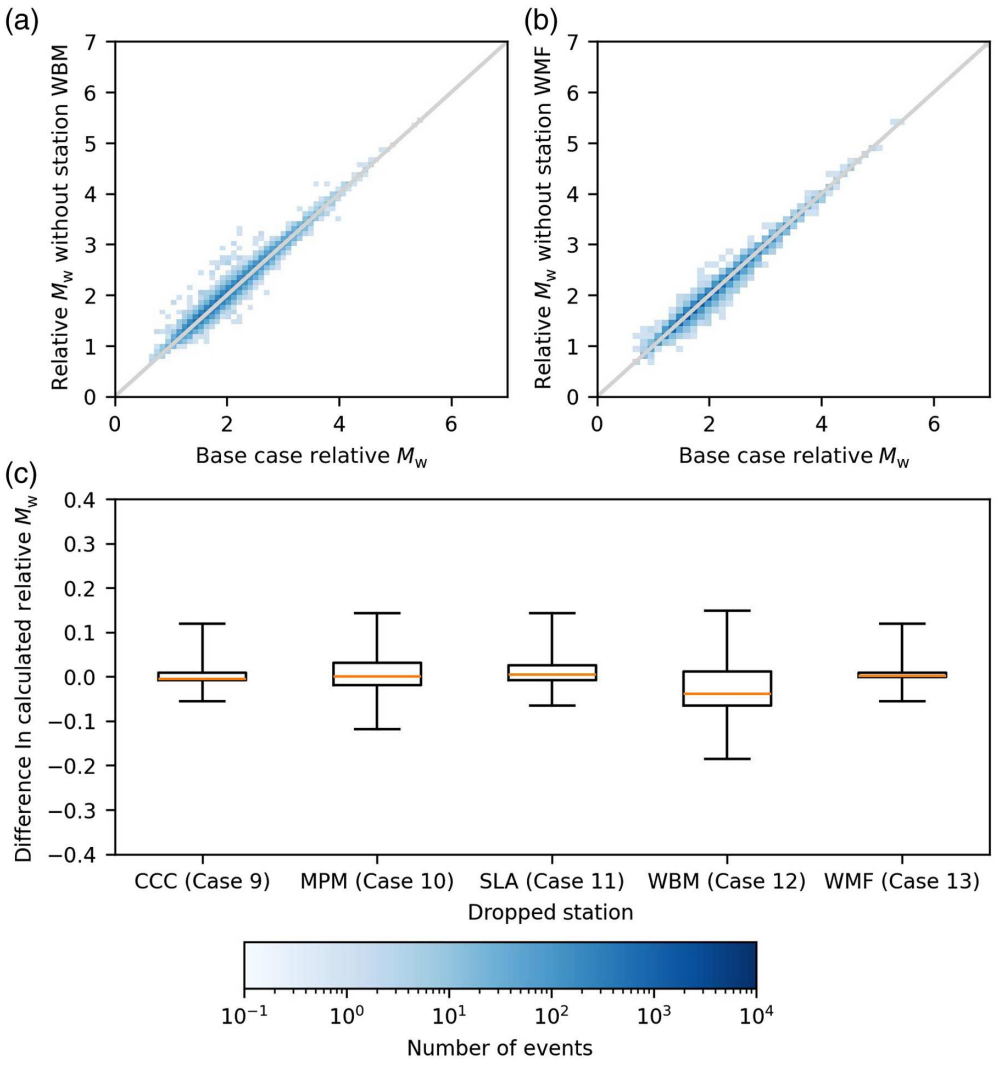

Figure 5. (a,b) Comparison between base-case M_w results and M_w results after a particular station has been excluded from the inversion. (c) Box limits represent the first and third quartile for the difference between base-case M_w and dropped station M_w. The orange line represents the median value. Whiskers represent the limits of the data points that are outside of the 95% interval. The color version of this figure is available only in the electronic edition.

that the exclusion of a particular station induces, we also note that in every case, at least 95% of the magnitudes have a difference of < 0.2 magnitude units from the base case, suggesting that the exclusion of any one station does not affect the results significantly. Despite this we still encourage future users of this method to consider a station configuration that includes as much azimuthal coverage as is practical with the available stations.

In addition, we examine the potential for measuring relative M_w from a single station (cases 14–18), which may be useful for a seismic region with low station coverage such as the central United States (Fig. 6). For stations MPM, SLA, and WBM, 95% of events have a magnitude difference less than 0.5 magnitude units from the base case. A relative M_w inversion using only station SLA shows the smallest difference from the base-case results. However, for an inversion in which we only use station WMF, 50% of events still are less than 0.3 magnitude units from the base case. However, the 95% interval of events shows more significant differences between the base case and single-station cases. This suggests that the relative magnitude method is possible if only a single station is available. However, including more than a single station, preferentially at different azimuths, allows for better constraints on magnitudes for small events (M <3) and the potential to include more pairs of events based on the geometry of source-to-station paths.

Finally, we investigate the variability imposed when we change the number of minimum stations on which observations must be made for a particular event pair (Fig. 7). We observe that raising the number of stations required accepting an event pair significantly reduces the number of events that are recalculated and leads to similar horizontal lineations as those that were observed in the CC threshold cases. In addition, we find that the variability between base case and increased station cases for individual M_w measurements is mostly below 0.5 magnitude units. Therefore, we suggest that it is acceptable to use a small minimum number of stations so that a maximum number of events may be recalculated.

Frequency filtering

The final parameter we investigate is the band-pass filtering procedures. We compare three cases (22–24) to the base case in which waveforms are filtered between 0.5 and 12 Hz (Fig. 8). First, we reduce the lower limit of the band-pass filter to 0.1 Hz to reduce any potential saturation of large magnitude events (case 22). Then, we return the lower limit to 0.5 and raise the upper limit of the band-pass filter to 20 Hz to capture energy of smaller events with high-corner frequencies (case 23). Finally, we introduce a split frequency band in case 24 for which M <3.5 events are filtered with the 0.5–20 Hz frequency band while M >3.5.

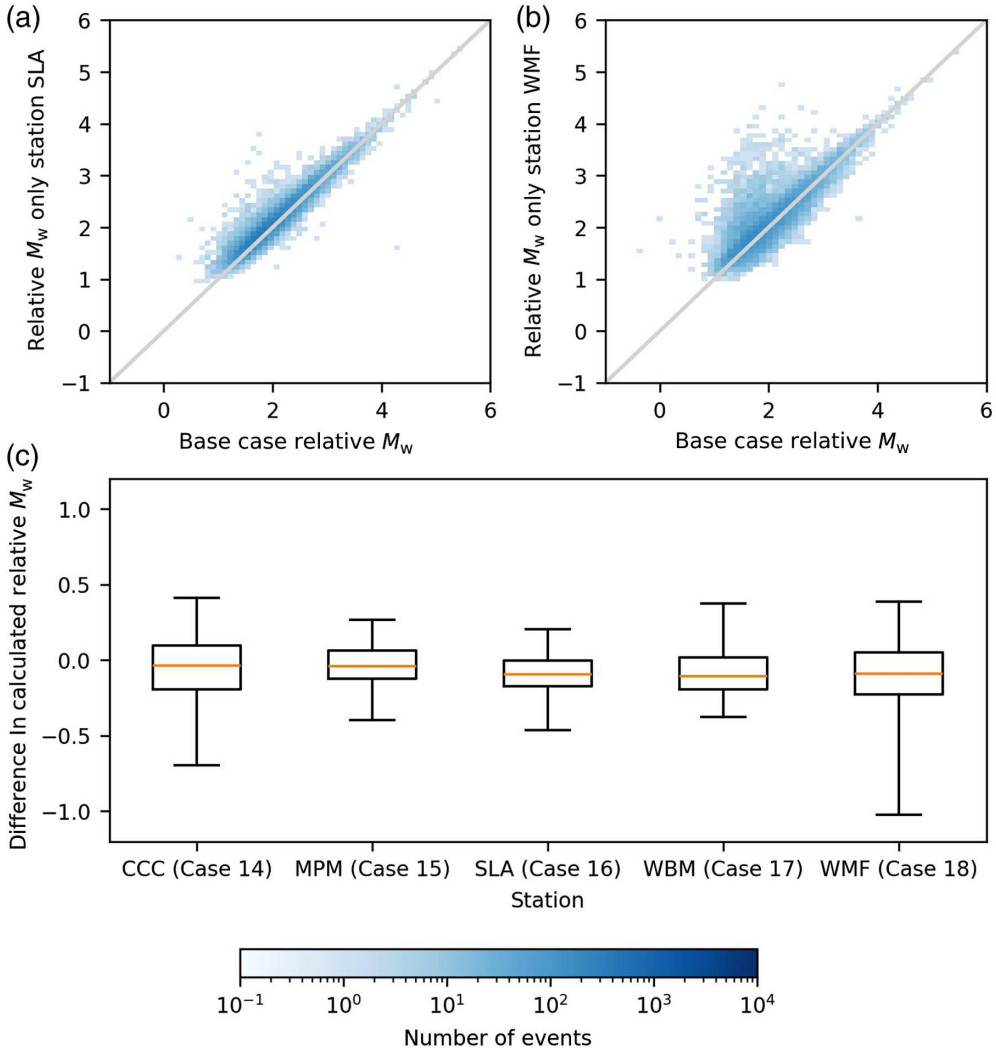

Figure 6. (a,b) Comparison between base-case M_w results and M_w results using only a single station. (c) Box limits represent the first and third quartile for the difference between base-case M_w and dropped station M_w. The orange line represents the median value. Whiskers represent the limits of the data points that are outside of the 95% interval. The color version of this figure is available only in the electronic edition.

Events are filtered with the 0.1–12 Hz frequency band to capture the effects of both the low- and high-frequency bands.

For the low-frequency band (case 20), we observe a turn in the distribution for which relative M_w is calculated to be nearly the same (between 1.5 and 2.5) for all M_L <2 events. This is a very sharp deviation from the base case for the smallest events. Although filtering at a low-frequency band is useful to prevent saturation for large events, we find that this allows low-frequency noise to contaminate the smallest events. Although these small events still pass the SNR threshold tests, their amplitudes are close to the low-frequency noise level, which results in overestimation of the relative M_w. A potential solution to this problem would be raising the SNR threshold to exclude these contaminated events. However, this would result in these small earthquakes simply being excluded from analysis rather than being calculated in a more ideal way.

When using a higher frequency passband (case 21), we observe a relationship between relative M_w and M_L that is more similar to the results in the base case.

However, only 8667 events have a relative M_w estimate. The inclusion of higher frequencies leads to lower correlation between waveform pairs due to increased waveform complexity. Thus, more waveform pairs are excluded from the analysis. Because the majority of events in this catalog have M <3.5, these effects also dominate in case 22 (the split frequency band). Therefore, we observe a similar set of results for cases 21 and 22.

Although amplitude saturation is a concern for catalogs that contain large earthquakes and one may feel compelled to use a low-frequency band to prevent amplitude saturation, we find that the best choice when using the relative magnitude method is a moderate frequency band that excludes as much high- and low-frequency noise as possible while still maintaining the integrity of the earthquake waveform. Further, the largest events in a catalog (M > ~5) are often excluded from the inversion regardless of small variations in the chosen passband due to increased waveform complexity and lack of events with similar magnitudes to form highly correlated pairs (Shelly *et al.*, 2016). Therefore, when working with catalogs that contain large earthquakes, we suggest not relying on the relative magnitude method and supplementing the relative M_w estimates with M_w derived from other methods such as waveform modeling and moment tensor inversion.

DISCUSSION AND CONCLUSIONS

Among all the parameters analyzed in this study, it is apparent that the choice of band-pass frequency range has the largest influence on the final results of the relative magnitude method in part because the influence of this parameter is extended to the other aspects of the analysis. If we choose a wide frequency band

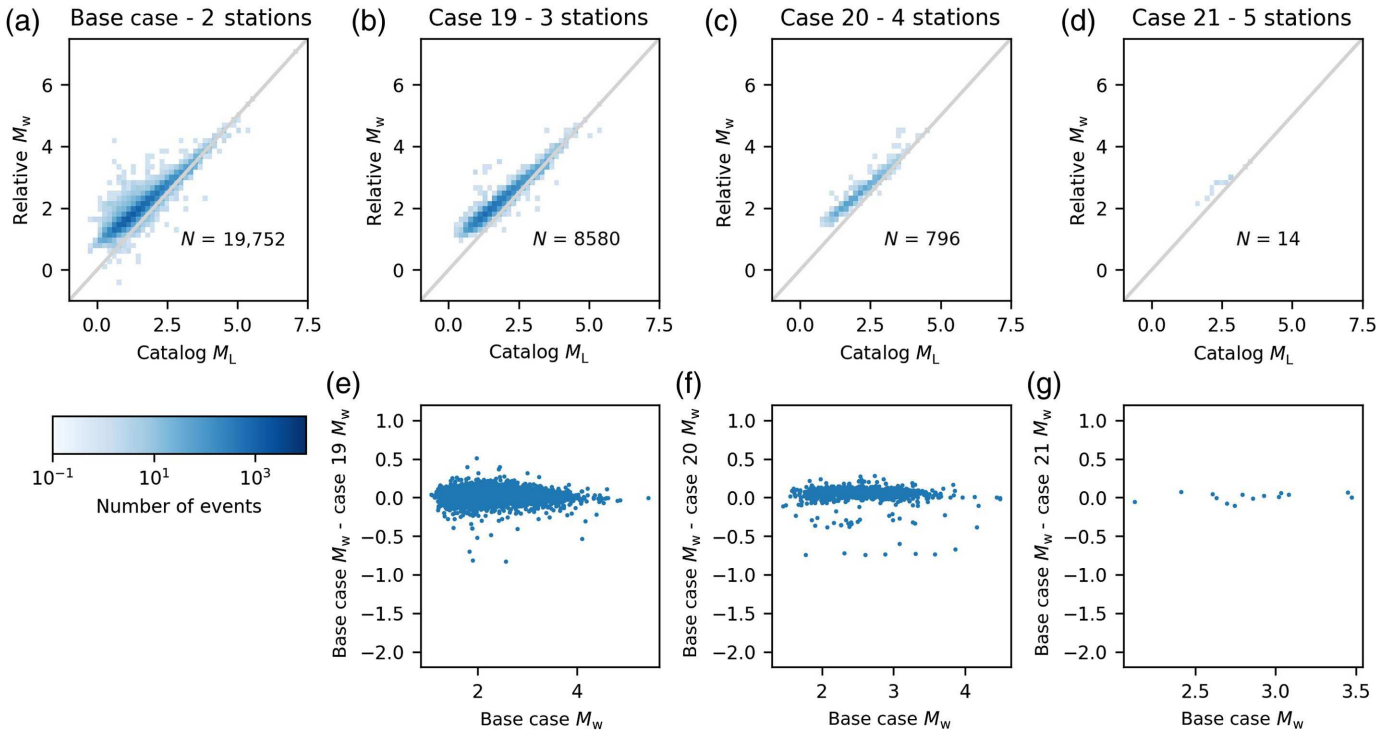

Figure 7. (a–d) Relative M_w results compared to M_L from the Shelly (2020) catalog for the base case (two stations per event pair), case 19 (three stations per event pair), case 20 (four stations per event pair), and case 21 (five stations per event pair). (e–g) Difference between base-case M_w results and results in each new case for the same event. The color version of this figure is available only in the electronic edition.

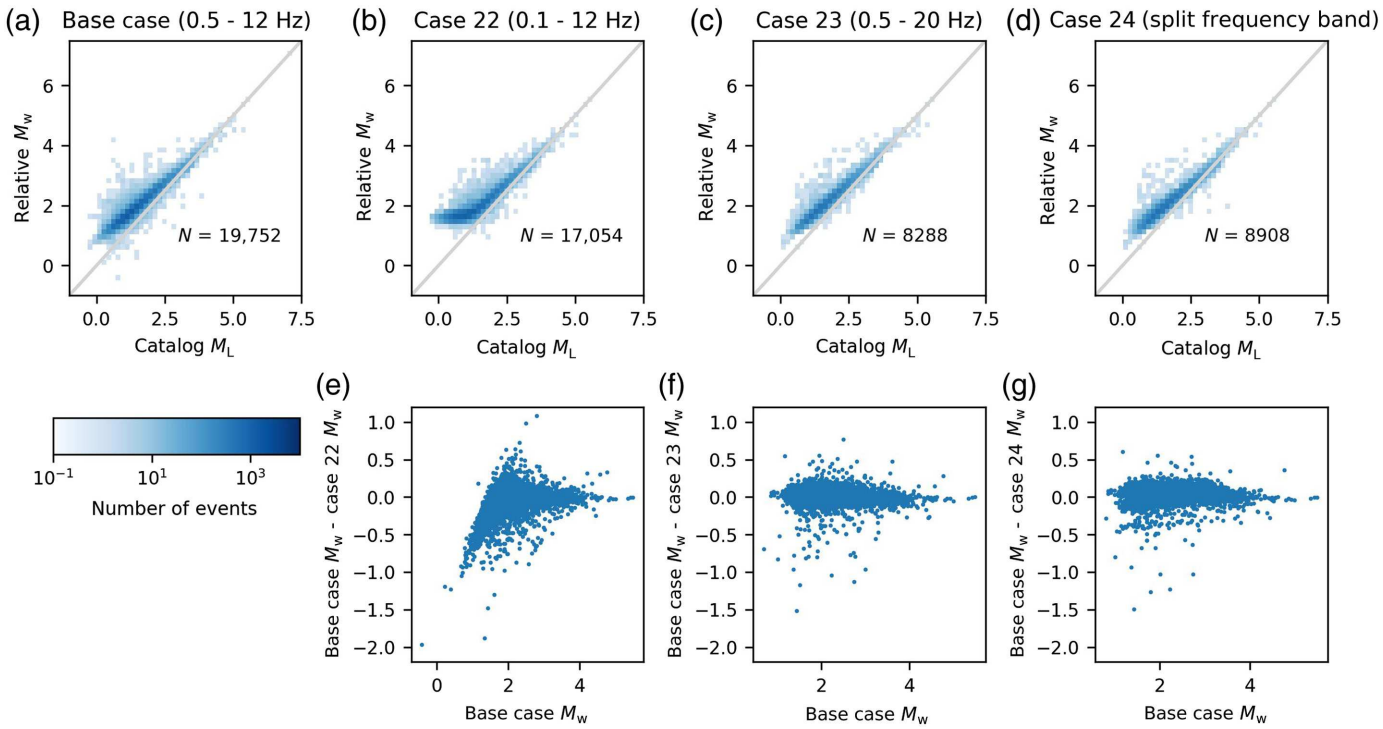

Figure 8. (a–d) Relative M_w results compared to M_L from the Shelly (2020) catalog for (a) the base case (0.5–12 Hz), (b) the low-frequency case (0.1–12 Hz), (c) the high-frequency case (0.5–20 Hz), and (d) the split frequency band case (M <3.5: 0.1–12 Hz, M >3.5: 0.5–20 Hz). (e–g) Difference between base-case M_w results and results in each case for the same event. The color version of this figure is available only in the electronic edition.

that contains more noise, then SNR and CC will be affected or need to be preemptively changed accordingly. This is particularly true for small (M <2) events. Future users of this method should carefully consider the frequency band that is most appropriate for the individual region and magnitude range. However, we suggest filtering procedures that prioritize signal from small magnitude events because the reduced number and inherent waveform complexity of large magnitude events means that they influence the results of the inversion less than the small to moderate events. In addition, M_w for large events may be measured using other common methods, and there are limited methods that may calculate M_w for events with M <3.

Apart from the frequency band variations, we find that slight changes in other parameters explored in this study—such as SNR, CC, and station selection—have minimal influence on the results of the relative M_w estimates. Approximately 95% of events in each scenario exhibit differences of less than 0.5 magnitude units from the base-case results except for two cases (14 and 18) for which only one station was used to recalculate magnitudes. This is a similar if not better level than the variability between different local magnitudes estimates for the same event (Shelly *et al.*, 2022; Gable and Huang, 2024a). Therefore, these parameters may be adjusted based on the needs and available resources of the user. For example, low SNR or CC threshold values will allow the user to establish estimates of M_w for many events, but in doing so the user may be sacrificing the potential accuracy of the magnitudes. Conversely, raising the SNR and CC thresholds enhances the potential for precise measurements of amplitude ratio, which consequently improves the magnitude difference. However, this sacrifices the number of resulting magnitudes. Users should also consider the available computational resources when making decisions regarding SNR and CC thresholds. The relative magnitude method is time intensive and computationally more expensive than traditional magnitude measurement methods. Therefore, as more events and more stations are included, more computational resources will be required. However, this method reduces the need for human interaction and does not require analysts to manually approve magnitude measurements. Nevertheless, we recommend that the highest level of accuracy within practical resource constraints should be strived for in future relative magnitude studies.

This study aims to mitigate potential error stemming from subjective decision making during the relative magnitude method. However, there are other potential sources of bias that arise from this method that should be investigated further. One factor is the window length of waveforms used for observations. Some studies, including this one, focus on specific segments of the waveform whereas others employ full-waveform amplitude analysis (Gable and Huang, 2024a). The length of the time window may affect the type of waves being measured and may influence the correlation between pairs of events.

Moreover, the optimal number of station measurements necessary to validate an event pair should also be investigated further. Not instituting a minimum number of stations allows for more event pairs to be included but sacrifices accuracy as more measurements will effectively average out more random error. However, although more stations may be useful to include more pairs of events, we must weigh the increased computational workload of including more stations against the perceived benefit of more observations. Here, we show that measurements made on five stations do not show much variability from measurements made on as little as two stations for the same event.

Finally, the minimum number of independently estimated events required for adequate calibration is an important control on the final absolute magnitudes, which we do not investigate further here. Theoretically, more calibration events would allow for better constraints on the relative magnitudes. However, we do not investigate this parameter here because the number of moment magnitude estimates available for the Ridgecrest sequence is very small compared to the size and magnitude range of the available catalog. Thus, we do not have very much leeway to vary the number of calibration events. In addition, we do not have any moment magnitude estimates for events below M 3.2 to evaluate the necessary magnitude range and scaling of calibration events. Future work may seek to independently establish a larger number of moment magnitude estimates for a wider range of magnitudes to investigate this. Current and future community work on standardizing source parameters for the Ridgecrest sequence may make this possible (Baltay *et al.*, 2024).

In summary, this study provides a method to accurately characterize earthquake magnitude without the need for the empirical distance and attenuation relationships or long-period waveforms that are currently required by common magnitude calculation methods. We establish a methodology for the relative magnitude method and investigate the variability that certain input parameters may impose on the magnitude results to make recommendations for future users. Although we acknowledge that this method may introduce slight biases that are inherent in the subjective decision making, we show that it is able to establish both local and moment magnitudes for many events in the Ridgecrest sequence in a way that is transportable to other geologic settings. Of most importance is the ability to establish moment magnitude estimates for small events (M <3) that are not routinely available using current methods. These results offer insights into the evolution of the Ridgecrest sequence and allow for further investigation into earthquake sources processes and seismic hazard in southern California.

DATA AND RESOURCES

Waveforms used in this study were downloaded from the Southern California Earthquake Data Center (SCEDC) using the International Federation of Digital Seismograph Networks (FDSN) Dataselect webservice (https://service.scedc.caltech.edu/fdsnws/dataselect/1/, last accessed October 2023) and were produced from stations in the Southern California Seismic Network (CI, stations CCC, MPM, SLA, WBM, and

WMF, doi: 10.7914/SN/CI). The Southern California Seismic Network (SCSN) earthquake catalog used here was also downloaded from the SCEDC (https://service.scedc.caltech.edu/eq-catalogs/date_mag_loc.php, last accessed October 2023). Other earthquake catalogs were obtained from published sources listed in references. Maps were prepared with Generic Mapping Tools (GMT; Wessel *et al.* 2019). The least-squares inversion and orthogonal regressions were determined using the Python–SciPy computing package (https://docs.scipy.org/doc/scipy/reference/odr.html and https://docs.scipy.org/doc/scipy/reference/generated/scipy.sparse.linalg.lsqr.html, respectively, last accessed June 2024). The catalog of relative M_w and M_L estimates presented in this article is available on the University of Michigan Deep Blue Archive (Gable and Huang 2024b). The supplemental material contains Figures S1–S4 showing representative examples of waveforms used in this study.

DECLARATION OF COMPETING INTERESTS

The authors acknowledge that there are no conflicts of interest recorded.

ACKNOWLEDGMENTS

The authors would like to thank Editor Annemarie Baltay as well as reviewers Katherine Whidden and Jonas Kintner for their incredibly helpful comments that have contributed to improving this article. In addition, the authors would like to thank David Shelly, Justin Rubinstein, and Xiaowei Chen for helpful discussion regarding the methodology and application of this method in other regions, and Caleb Shook for helpful discussion and suggestions regarding computational methods. The authors also recognize funding from National Science Foundation (NSF) Grant EAR-2315814 for supporting this research.

REFERENCES

Atkinson, G. M., D. W. Greig, and E. Yenier (2014). Estimation of moment magnitude (M) for small events (M<4) on local networks, *Seismol. Res. Lett.* **85,** 1116–1124, doi: 10.1785/0220130180.

Baltay, A., R. E. Abercrombie, S. Chu, and T. Taira (2024). The SCEC/USGS community stress drop validation study using the 2019 Ridgecrest earthquake sequence, *Seismica Reports*, doi: 10.26443/seismica.v3i1.1009.

Bethmann, F., N. Deichmann, and P. M. Mai (2011). Scaling relations of local magnitude versus moment magnitude for sequences of similar earthquakes in Switzerland, *Bull. Seismol. Soc. Am.* **101,** 575–534, doi: 10.1785/0120100179.

Bindi, D., D. Spallarossa, M. Picozzi, D. Scafidi, and F. Cotton (2018). Impact of magnitude selection on aleatory variability associated with ground-motion prediction equations: Part I - local, energy, and moment magnitude calibration and stress-drop variability in Central Italy, *Bull. Seismol. Soc. Am.* **108,** 1427–1442, doi: 10.1785/0120170356.

Bindi, D., R. Zaccarelli, and S. R. Kotha (2021). Local and moment magnitude analysis in the Ridgecrest region, California: Impact on interevent ground-motion variability, *Bull. Seismol. Soc. Am.* **111,** 339–355, doi: 10.1785/0120200227.

Castellaro, S., F. Mulargia, and Y. Y. Kagan (2006). Regression problems for magnitudes, *Geophys. J. Int.* **165,** 913–930, doi: 10.1111/j.1365-246X.2006.02955.x.

Chen, X., J. Haffener, T. H. W. Goebel, X. Meng, Z. Peng, and J. C. Chang (2018). Temporal correlation between seismic moment and injection volume for an induced earthquake sequence in Central Oklahoma, *J. Geophys. Res.* **123,** 3047–3064, doi: 10.1002/2017JB014694.

Cheng, Y., and Y. Ben-Zion (2020). Variations of earthquake properties before, during, and after the 2019 M7.1 Ridgecrest, CA, earthquake, *Geophys. Res. Lett.* **47,** e2020GL089650, doi: 10.1029/2020GL089650.

Cheng, Y., X. Wang, Z. Zhan, and Y. Ben-Zion (2021). Isotropic source components of events in the 2019 Ridgecrest, California, earthquake sequence, *Geophys. Res. Lett.* **48,** doi: 10.1029/2021GL094515.

Cleveland, K. M., and C. J. Ammon (2015). Precise relative earthquake magnitudes from cross correlation, *Bull. Seismol. Soc. Am.* **105,** 1792–1796, doi: 10.1785/0120140329.

Deichmann, N. (2006). Local magnitude, a moment revisited, *Bull. Seismol. Soc. Am.* **96,** 1267–1277, doi: 10.1785/0120050115.

Deichmann, N. (2017). Theoretical basis for the observed break in M_L/M_W scaling between small and large earthquakes, *Bull. Seismol. Soc. Am.* **107,** 505–520, doi: 10.1785/0120160318.

Edwards, B., B. Allmann, D. Fäh, and J. Clinton (2010). Automatic computation of moment magnitudes for small earthquakes and the scaling of local to moment magnitude, *Geophys. J. Int.* **183,** 407–420.

Gable, S. L., and Y. Huang (2024a). New estimates of magnitude-frequency distribution and b-value using relative magnitudes for the 2011 Prague, Oklahoma earthquake sequence, *J. Geophys. Res.* **129,** e2023JB026455, doi: 10.1029/2023JB026455.

Gable, S. L., and Y. Huang (2024b). Relative moment magnitude (Mw) estimates for the 2019 Ridgecrest, CA sequence [Data set], University of Michigan, Deep Blue Data, doi: 10.7302/cmqq-9e09

Gasperini, P., B. Lolli, and G. Vannucci (2013). Empirical calibration of local magnitude data sets versus moment magnitude in Italy, *Bull. Seismol. Soc. Am.* **103,** 2227–2246, doi: 10.1785/0120120356.

Hanks, T. C., and D. M. Boore (1984). Moment-magnitude relations in theory and practice, *J. Geophys. Res.* **89,** 6229–6235.

Herrmann, M., and W. Marzocchi (2021). Inconsistencies and lurking pitfalls in the magnitude frequency distribution of high-resolution earthquake catalogs, *Seismol. Res. Lett.* **92,** 909–922, doi: 10.1785/0220200337.

Holt, J., K. M. Whidden, K. D. Koper, K. L. Pankow, K. Mayeda, J. C. Pechmann, B. Edwards, R. Gök, and W. R. Walter (2021). Toward robust and routine determination of m_w for small earthquakes: Application to the 2020 M_W 5.7 Magna, Utah, seismic sequence, *Seismol. Res. Lett.* **92,** 725–740, doi: 10.1785/0220200320.

Howell, B. F. (1981). On the saturation of earthquake magnitudes, *Bul. Seismol. Soc. Am.* **71,** 1401–1422.

Huang, Y., and G. C. Beroza (2015). Temporal variation in the magnitude-frequency distribution during the Guy-Greenbrier earthquake sequence, *Geophys. Res. Lett.* **42,** 6639–6646, doi: 10.1002/2015GL065170.

Hutton, L. K., and D. M. Boore (1987). The M_L scale in Southern California, *Bul. Seismol. Soc. Am.* **77,** 2074–2094.

Kanamori, H. (1977). The energy release in great earthquakes, *J. Geophys. Res.* **82,** 2981–2987.

Kintner, J. A., C. J. Ammon, K. M. Cleveland, and M. Herman (2018). Rupture processes of the 2013-2014 Minab earthquake sequence, Iran, *Geophys. J. Int.* **213,** 1898–1911.

Kintner, J. A., C. J. Ammon, K. Homman, and A. Nyblade (2020). Precise relative magnitude and relative location estimates of

low-yield industrial blasts in Pennsylvania, *Bull. Seismol. Soc. Am.* **110,** no. 1, 226–240.

Kuehn, N. M., and N. A. Abrahamson (2018). The effect of uncertainty in predictor variables on the estimation of ground-motion prediction equations, *Bull. Seismol. Soc. Am.* **108,** 358–370, doi: 10.1785/0120170166.

Liu, C., T. Lay, E. E. Brodsky, K. Dascher-Cousineau, and X. Xiong (2019). Coseismic rupture process of the large 2019 Ridgecrest earthquakes from joint inversion of geodetic and seismological observations, *Geophys. Res. Lett.* **46,** 11,820–11,829, doi: 10.1029/2019GL084949.

Liu, M., M. Zhang, W. Zhu, W. L. Ellsworth, and H. Li (2020). Rapid characterization of the July 2019 Ridgecrest, California, earthquake sequence from raw seismic data using machine-learning phase picker, *Geophys. Res. Lett.* **47,** e2019GL086198 , doi: 10.1029/2019GL086189.

Ponti, D. J., J. L. Blair, C. M. Rosa, K. Thomas, A. J. Pickering, A. Morelan, and T. Dawson (2020). Digital datasets documenting surface fault rupture and ground deformation features produced by the Ridgecrest M6.4 and M7.1 earthquake sequence of July 4 and 5, 2019, *U.S. Geol. Surv. Data Release*, doi: 10.5066/P9BZ5IJ9.

Richter, C. F. (1935). An instrumental earthquake magnitude scale, *Bull. Seismol. Soc. Am.* **25,** 1–32.

Ristau, J. (2009). Comparison of magnitude estimates for New Zealand earthquakes: Moment magnitude, local magnitude, and teleseismic body-wave magnitude, *Bull. Seismol. Soc. Am.* **99,** 1841–1852, doi: 10.1785/0120080237.

Ristau, J., G. C. Rogers, and J. F. Cassidy (2003). Moment magnitude – local magnitude calibration for earthquakes off Canada's west coast, *Bull. Seismol. Soc. Am.* **93,** 2296–2300, doi: 10.1785/0120030035.

Ross, Z. E., Y. Ben-Zion, M. C. White, and F. L. Vernon (2016). Analysis of earthquake body wave spectra for potency and magnitude values: implications for magnitude scaling relations, *Geophys. J. Int.* **207,** 1158–1164, doi: 10.1093/gji/ggw327.

Savage, M. K., and J. G. Anderson (1995). A local-magnitude scale for the western great basin-Eastern Sierra Nevada from synthetic Wood-Anderson seismograms, *Bull. Seismol. Soc. Am.* **85,** 1236–1243.

Schaff, D. P., and P. G. Richards (2014). Improvements in magnitude precision, using the statistics of relative amplitudes measured by cross correlation, *Geophys. J. Int.* **197,** 335–350, doi: 10.1093/gji/ggt433.

Shelly, D. R. (2020). A high-resolution seismic catalog for the initial 2019 Ridgecrest earthquake sequence: Foreshocks, aftershocks, and faulting complexity, *Seismol. Res. Lett.* **91,** 1971–1978, doi: 10.1785/0220190309.

Shelly, D. R., W. L. Ellsworth, and D. P. Hill (2016). Fluid faulting evolution in high definition: Connecting fault structure and frequency-magnitude variations during the 2014 Long Valley Caldera, California earthquake swarm, *J. Geophys. Res.* **121,** 1778–1795, doi: 10.1002/2015JB012719.

Shelly, D. R., K. Mayeda, J. Barno, K. M. Whidden, M. P. Moschetti, and A. L. Llenos (2022). A big problem for small earthquakes: Benchmarking routine magnitudes and conversion relationships with coda envelope-derived M_W in Southern Kansas and Northern Oklahoma, *Bull. Seismol. Soc. Am.* **112,** 210–225, doi: 10.1785/0120210115.

Trugman, D. T. (2020). Stress-drop and source scaling of the 2019 Ridgecrest, California, earthquake sequence, *Bull. Seismol. Soc. Am.* **110,** 1859–1871, doi: 10.1785/0120200009.

Urlhammer, R. A., M. Hellweg, K. Hutton, P. Lombard, A. W. Walters, and E. Hauksson (2011). California integrated seismic network (CISN) local magnitude determination in California and vicinity, *Bull. Seismol. Soc. Am.* **101,** 2685–2693, doi: 10.1785/0120100106.

Waldhauser, F., and W. L. Ellsworth (2000). A double-difference earthquake location algorithm method and application to the Northern Hayward Fault, California, *Bull. Seismol. Soc. Am.* **90,** 1353–1368, doi: 10.1785/0120000006.

Wessel, P., J. F. Luis, L. Uieda, R. Scharroo, F. Wobbe, W. H. F. Smith, and D. Tian (2019). The Generic Mapping Tools Version 6, *Geochem. Geophys. Geosys.* **20,** 5556–5564, doi: 10.1029/2019GC008515.

Woessner, J., and S. Weimer (2005). Assessing the quality of earthquake catalogues: estimating the magnitude of completeness and its uncertainty, *Bull. Seismol. Soc. Am.* **95,** 684–698, doi: 10.1785/0120040007.

Manuscript received 17 June 2024
Published online 12 December 2024